NUCLEAR INSTRUMENTS AND METHODS 165 (1979) 217-224; © NORTH-HOLLAND PUBLISHING CO.

THE RESPONSE FUNCTION OF ORGANIC SCINTILLATORS TO FAST NEUTRONS

M. ANGHINOLFI, G. RICCO, P. CORVISIERO and F. MASULLI

Istituto Nazionale di Fisica Nucleare, Sezione di Genova, Istituto di Scienze Fisiche dell'Università, Genova, Italy

Received 28 May 1979

Neutron response functions of cylindrical organic scintillators in the energy range $1 \leq E_n \leq 200$ MeV have been evaluated using a Monte Carlo program.

The effects of the angular distribution in H and ^{12}C and the contribution of the direct $^{12}C(\bar{n}, p)$ channel at high energies have been investigated.

The obtained results have been compared with the available experimental response functions in NE102A, NE213 and NE218.

1. Introduction

Organic scintillators are widely used in experimental physics as neutron detectors. Their fast response, high efficiency and relatively low cost make them still nowadays an important tool in intermediate and high energy physics experiments[1]). The response function $P_N(E, L)$, i.e. the pulse height (L) distribution corresponding to N monochromatic neutrons incident in the scintillator volume, must be accurately evaluated as a function of the neutron energy E and detector geometry.

Monte Carlo routines[2-4]) have been proposed to calculate the percent efficiency

$$\varepsilon(E) = \frac{1}{N} \int_{L_{th}}^{L_{max}} P_N(E, L)\, dL$$

for discrete values of the threshold level L_{th}. Most calculations were performed assuming a fixed scintillator composition and low neutron energy ($E \leqslant 20$ MeV): in these conditions the efficiency curves generally result in fair agreement with the existing experimental data, but only in a few cases the whole response function was reported[4,17]). At higher energies the problem is more complicated: the total neutron cross sections in H and C nuclei are plotted in fig. 1a as a function of the incident neutron energy. Above 10 MeV the neutron–carbon interaction becomes stronger than the better known neutron–hydrogen elastic cross section. The simulation of the neutron random walk in the scintillator at high energies requires therefore a complete description of all the involved elastic and inelastic neutron–carbon channels (fig. 1b) and the computed response functions become more sensitive to the details of the nuclear reactions and to the uncertainties on the corresponding cross section data. This sensitivity is reduced in the efficiency ε, particularly at low threshold values L_{th}, allowing an easier agreement with experimental data, provided that total cross sections are correctly evaluated in each reaction channel[5]). The aim of the present work is a complete calculation of response functions $P_N(E, L)$ in the neutron energy range

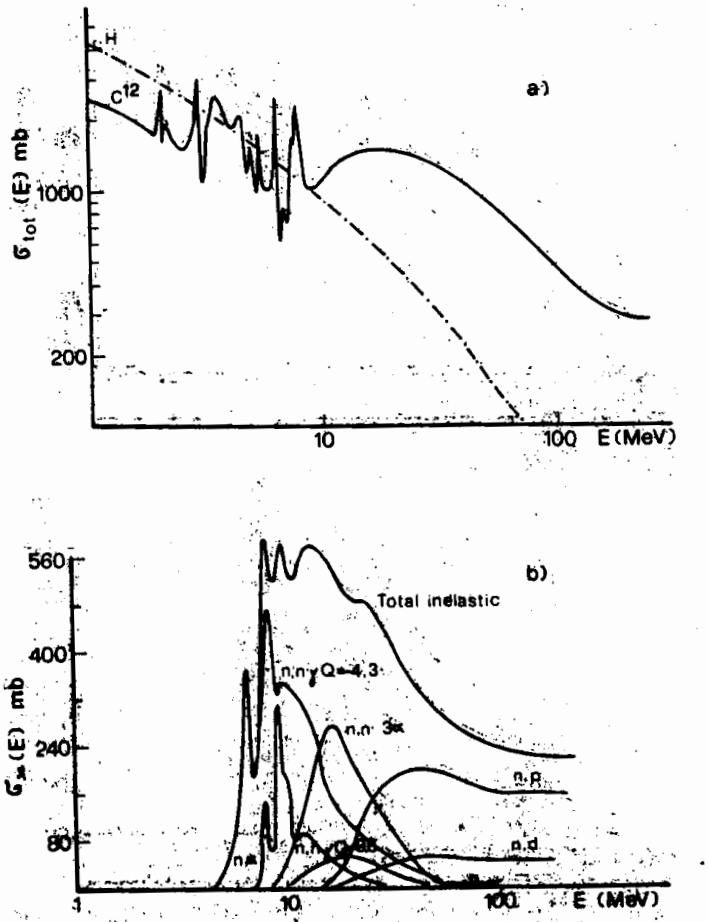

Fig. 1. (a) Total neutron cross sections in H and ^{12}C. (b) Inelastic neutron–carbon cross sections. Data points are taken from the compilation of ref. 5.

$1 \leqslant E \leqslant 200$ MeV for different scintillator sizes and compositions. A standard Monte Carlo method has been used to simulate the history of neutrons on their way through the detector, but particular attention has been devoted to the detailed description of total and differential cross sections at high energies. In particular,

- The elastic and inelastic differential cross sections $d\sigma/d\Omega$ in H and C nuclei have been interpolated from the existing data. Above 10 MeV the neutron–carbon angular distributions show a pronounced forward shift which is not reproduced by the currently used analytic expressions[3]).
- A physical description has been attempted of the $^{12}C(n, p)$ and $^{12}C(n, d)$ reactions, i.e. the two- and few-body disintegration of ^{12}C leading to a proton or a deuteron in the final state. This process, which becomes above 30 MeV the most important neutron detection channel in the scintillator (fig. 1b), has been scarcely investigated in the existing literature.
- Edge effects on the energy loss of charged particles in the scintillator have been taken into account. Again these effects give non-negligible contributions, at least for medium size detectors, at neutron energies above 100 MeV (fig. 7).
- In order to have a large number of experimental data available a systematic investigation has been performed of response functions and efficiencies in the most widely used detectors, typically Nuclear Enterprise NE102A, NE213 and NE218, whose compositions are reported in table 1. The Monte Carlo program and the data compilation are described in sect. 2 and the obtained results are discussed in sect. 3.

2. General outline of the program

The block diagram of the program, reported in fig. 2, has been schematically divided into three parts:

a) *Geometrical routines* concerning the neutron path from the source up to the detector. Neutrons, generated from randomly chosen points in the source area with uniform angular distribution inside the allowed solid angle $\Delta\Omega$ and given energy spectrum $n(E)$, have been followed up to the first interaction point at the distance

$$r = -\ln q/[N_C\sigma^C_{tot}(E) + N_H\sigma^H_{tot}(E)]$$

inside the scintillator, where q is a random number in the 0–1 interval and $\sigma^{H(C)}(E)$ are the total cross sections of fig. 1a. The detector has a cylindrical shape with "end on" incidence and different geometries like point source, parallel beam and extended reaction target are allowed.

b) *Interaction routines* which select the neutron–nucleus interaction and the final state parameters. The target nucleus (H or ^{12}C) and the reaction channel $\bar{x}$ have been determined by the well known Monte Carlo rules[8]):

$$q_1 \gtrless \frac{N_H\sigma^H_{tot}(E)}{N_H\sigma^H_{tot}(E) + N_C\sigma^C_{tot}(E)},$$

$$q_2 \gtrless \frac{\sum_{x \neq \bar{x}} \sigma^{H(C)}_x E)}{\sum_x \sigma^{H(C)}_x(E)}, \qquad (1)$$

where $N_{H(C)}$ is the number of H(C) nuclei per cm^3, $\sigma_{tot}(E)$ the total neutron cross section and $\sigma_x(E)$ the channel cross section. The cross section curves, reported in fig. 1, have been interpolated from the data compilation of Del Guerra[5]).

The kinematic parameters, namely energy $E_{\bar{x}}$ and angle $\vartheta_{\bar{x}}$ of the final reaction products in the $\bar{x}$ channel are chosen using differential cross sections and random number generation:

$$q_1 = \frac{\int_0^{\vartheta_{\bar{x}}} (d\sigma/d\vartheta)\, d\vartheta}{\int_0^{2\pi} (d\sigma/d\vartheta)\, d\vartheta}, \quad q_2 = \frac{\int_0^{E_{\bar{x}}} (d\sigma/dE)\, dE}{\int_0^{E_{max}} (d\sigma/dE)\, dE}. \qquad (2)$$

TABLE 1

Composition of main organic scintillators.

Type	Density (g/cm^3)	N_H H atoms/cm^3 (cm^{-3})	N_C C atoms/cm^3 (cm^{-3})	H/C ratio	Light output (% Antrac.)
NE102A	1.032	5.82×10^{22}	4.78×10^{22}	1.104	65
NE213	0.874	4.82×10^{22}	3.98×10^{22}	1.213	78
NE218	0.879	5.10×10^{22}	3.99×10^{22}	1.28	70

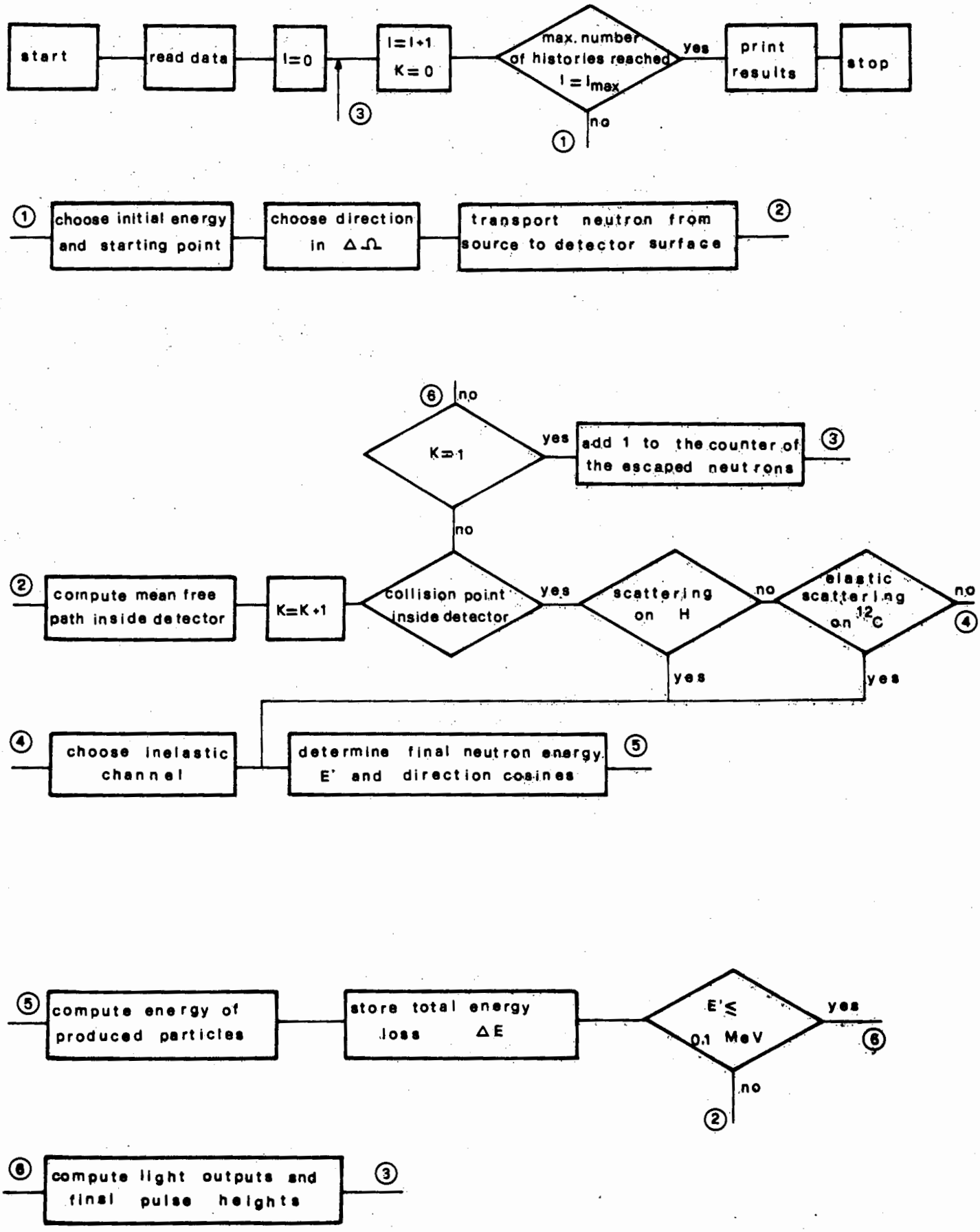

Fig. 2. Block diagram of the Monte Carlo program.

TABLE 2

Elastic angular distribution coefficients in the c.m. system for the H(n, n)H reaction.

Energy (MeV)	14.	22.5	27.5	32.5	37.5	52.5	70.	90.	156.	260.
A_0	55.7	33.8	27.9	23.4	19.2	13.2	8.1	6.3	3.9	2.8
A_1	—	−0.1	0.07	2.3	1.1	0.84	0.5	−0.5	−1.3	−0.68
A_2	—	1.8	2.7	2.9	3.2	4.3	5.2	4.7	3.7	3.1
A_3	—	0.16	−0.2	−2.	−1.2	−0.1	−0.4	0.15	0.3	−0.78
A_4	—	0.23	0.02	1.1	0.2	1.1	0.5	1.6	1.3	0.98

TABLE 3

a) Elastic and inelastic angular distribution coefficients in the c.m. system for the $^{12}C(n, n)^{12}C$ reaction.

Energy (MeV)	2.02	2.15	2.65	2.76	2.84	2.95	3.01	3.05	3.25	3.65	3.76	4.21	4.73	5.
A_0	144.	145.	133.	157.	164.	223.	115.	109.	155.	194.	183.	160.	108.	81.
A_1	16.3	−21.2	6.8	−22.5	−6.	−16.8	−2.2	−25.5	−13.6	4.7	−3.	92.	102.	84.
A_2	33.9	49.9	116.6	162.6	190.1	393.	68.7	68.	261.	344.	314.	179.	89.	65.
A_3	−15.8	11.4	−7.	−20.8	6.7	−14.	16.3	−14.2	6.2	14.3	31.	75.	79.	92.
A_4	5.1	4.4	−11.1	−14.	−12.	−15.6	6.8	0.2	−12.7	22.5	28.4	52.6	40.	53.
A_5	–	–	–	–	–	–	–	–	–	–	–	–	–	–
A_6	–	–	–	–	–	–	–	–	–	–	–	–	–	–

Energy (MeV)	6.	6.3	7.0	7.2	7.73	8.2	9.	12.	15.8	20.	95.	136.	350.
A_0	64.	96.	45.	46.	90.	17.	−36.	−1.	17.8	19.6	–	–	–
A_1	36.	40.	33.2	50.	−14.6	−11.7	−137.	−52.	−2.2	21.3	–	–	–
A_2	41.	71.	13.7	25.	146.	7.	−85.	−30.	−6.8	3.2	–	–	–
A_3	60.	145.	30.	12.5	55.	36.2	10.	23.9	8.5	3.1	–	–	–
A_4	5.5	63.	15.2	6.1	60.	48.	6.1	24.	15.2	6.3	–	–	–
A_5	–	–	–	–	491.	627.	635.	569.	742.	1176.	1129.	1147.	959.
A_6	–	–	–	–	−9.8	−5.6	−3.4	−4.3	−7.2	−9.9	−33.	−49.	−84.

(b) Elastic and inelastic angular distribution coefficients in the c.m. system for the $^{12}C(n, n'\gamma)^{12}C$ reaction.

Energy (MeV)	6.	6.63	7.	7.73	8.2	9.	14.	16.7	19.4	96.	185.
A_0	18.1	27.4	14.8	30.1	39.2	22.1	18.4	12.1	–	–	–
A_1	3.3	1.6	−1.	−4.1	−13.6	0.4	14.9	9.2	–	–	–
A_2	4.	11.	6.	−1.9	33.4	18.6	22.7	12.	–	–	–
A_3	0.81	1.32	.15	–	−22.4	3.2	3.8	2.4	–	–	–
A_4	0.06	−.61	−3.36	–	–	2.6	3.7	−1.	–	–	–
A_5	–	–	–	–	–	–	–	–	31.5	17.6	8.8
A_6	–	–	–	–	–	–	–	–	−1.9	−6.7	−10.6

For a two-body reaction $n+T \rightarrow x+X$ only the angular distribution $d\sigma/d\Omega$ is required since kinetic energy E_x and emission angle ϑ_x are related by the kinematic expression[16]):

$$Q = M_n+M_T-M_x-M_X = \left(-1+\frac{M_n}{M_X}\right)E_n + \\ +\left(1+\frac{M_x}{M_X}\right)E_x - \frac{2}{M_X}\sqrt{(M_n M_x E_n E_x \cos\vartheta_x)}. \quad (3)$$

Unfortunately the experimental data on differential cross sections are still very fragmentary, particularly in the inelastic channels, and additional assumptions are often required. We shall therefore report a brief discussion of the angular and energy distributions adopted in this work.

H(n, n)H. The angular distribution in the c.m. system below 14 MeV is isotropic and shows a parabolic shape[9]) at higher energies. The existing data have been fitted by the sum of five Legendre polynomials

$$\frac{d\sigma}{d\Omega}(E_n) = \sum_{l=0}^{4} A_l P_l(\cos\vartheta_{c.m.}), \quad (4)$$

and the obtained coefficients A_l are listed in table 2. Points at intermediate energies have been obtained by linear interpolation.

$^{12}C(n, n)^{12}C$. The elastic cross section is isotropic in the c.m. system below 2 MeV and is well reproduced by expression (4) between 2 and 10 MeV (table 3). The fluctuating behaviour of the coefficients A_l as a function of the neutron energy is due to the existence of close resonances in this energy range (fig. 1a). Above 10 MeV the angular distribution exhibits a pronounced forward shift[7]) and the simple polynomial fit eq. (4) is no longer adequate. We have therefore introduced an additive exponential term, which becomes dominant at high energy (table 3).

$$\frac{d\sigma}{d\Omega} = \sum_{l=0}^{4} A_l P_l(\cos\vartheta_{c.m.}) + A_5 \exp[A_6(1-\cos\vartheta_{c.m.})]. \quad (5)$$

$^{12}C(n, n'\gamma)^{12}C$. Inelastic transitions have been systematically observed only to the final 4.43 MeV and 9.6 MeV levels in ^{12}C. The available data on the $Q = -4.43$ MeV transition show an angular distribution similar to the elastic one[10]). The seven parameter fit eq. (5) has therefore been used (table 3).

For the $Q = -9.6$ MeV transition only few data[10,11]) exist in the literature: the neutron angular distribution has at all energies the trapezoidal shape reported in fig. 3 together with the fitted values of the parameters. The scattered neutron energy is computed from eq. (3) using the proper Q-values. Following de-excitation of the nucleus γ-rays are emitted with angular distribution assumed equal, at all energies, to the value measured at 14 MeV[9]). The photon path has been followed and the energy lost by Compton and pair electrons stored.

$^{12}C(n, \alpha)^{9}Be$. The α-particle energy has been computed from eq. (3) assuming ^{9}Be in its ground state ($Q = -5.7$ MeV) and the angular distribution has been taken from ref. 12.

$^{12}C(n, n'3\alpha)$. The experimental results on this reaction have been fairly well reproduced[13]) assuming an isotropic angular distribution and four-particle phase space energy spectra $p(\varepsilon)d\varepsilon = A\sqrt{\varepsilon}(1-\varepsilon)^2 d\varepsilon$, where $\varepsilon = E/E^{max}$ is the ratio between the particle energy and its maximum value allowed by kinematics.

$^{12}C(n, p)$, $^{12}C(n, d)$. Under this name are generally classified the neutron induced reactions leading to a proton or a deuteron in the final state. The proton energy distribution, measured at $E = 56$ MeV [14]), exhibits discrete transitions to the g.s. and first excited states of ^{12}B from the two-body reaction $^{12}C(n, p)^{12}B$ * and a continuous spectrum, extending down to the experimental threshold, due to the open few-body disintegration channels[15]).

According to this result the proton energy distribution may be parametrized as the sum of a fast component $\delta_1(E_p)$ and a slow component $\delta_2(E_p)$,

$$p(E_p)dE_p = A[\delta_1(E_p) + h\delta_2(E_p)], \quad (6)$$

where

$$\delta_2(E_p) = \sqrt{\left(\frac{E_p}{E_p^{max}}\right)}\left(1-\frac{E_p}{E_p^{max}}\right)^2$$

is a four-body phase space and

$$\delta_1(E_p) = \frac{7.4}{(E_p-E_p^{max}+4.3)^2+13.7}$$

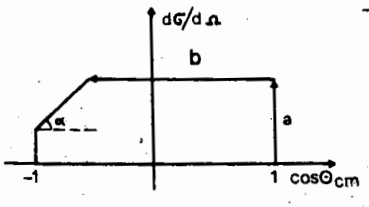

E(MeV)	a(mb)	b	tan(α)
14.	6.6	1.1	5.8
18.9	6.4	0.9	5.8
185.	1.7	0.1	5.8

Fig. 3. Angular distribution of the $^{12}C(n, n')^{12}C$ * (9.6 MeV) reaction at measured neutron energies E_n.

a two-body Lorentz spectrum covering an excitation energy range of 7.4 MeV fwhm in ^{12}B peaked on the 4.3 MeV level in qualitative agreement with the data[14]).

In eq. (6) A is a normalization factor E_p^{max} is the maximum (two-body) proton energy and $h(E)$ measures the relative strength of the two components which is supposed to be a function of the incident neutron energy E. Since experimental data at various energies are not presently available, it is convenient to leave h as a free parameter to be determined by the best fit procedure reported in the next section (table 4).

c) *Light output routines.* Every charged particle produces a light output which is non-linearly dependent on the particle mass, its energy loss E and the scintillator composition. This light output is generally expressed in MeV equivalent electron (Mee), i.e. the electron energy $L_k(E)$ which would produce the same amount of light as the particle K at energy E. The used values of the function $L_k(E)$ for different k particle masses in various scintillators are reported in fig. 4 as a function of the energy E. The total pulse height L (fig. 5) associated with the whole neutron path is given by $L = \sum_k L_k(E)$, where the sum runs all over the charged reaction products.

TABLE 4

Relative strength h of the direct $^{12}C(n, p)^{12}B$ reaction.

Energy (MeV)	13.6	30.	45.	⩾60.
h	0.	0.3	0.38	0.24

The incident neutron history has been followed up to a final energy 0.1 MeV or, alternatively, to escape from the scintillator volume. For each path the energy E released to ionizing particles has been stored and the corresponding ionization range computed. For ranges $R(E)$ extending outside the scintillator boundary the internal R_{int} and external R_{ext} path lengths have been stored. The escaped energy

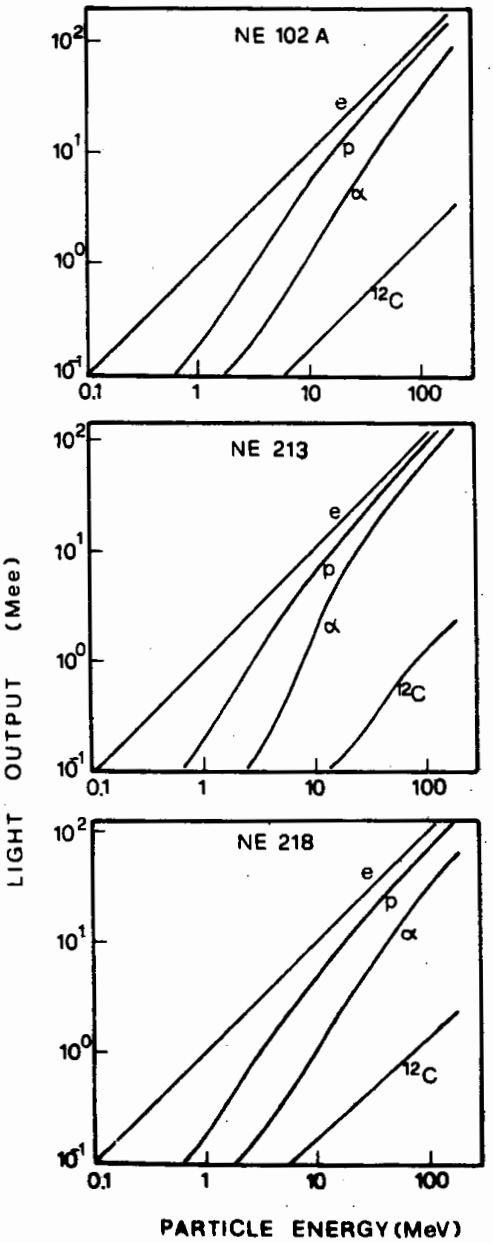

Fig. 4. Light outputs in MeV electron equivalent for NE102 A [3]), NE213 [17]) and NE218 [18]).

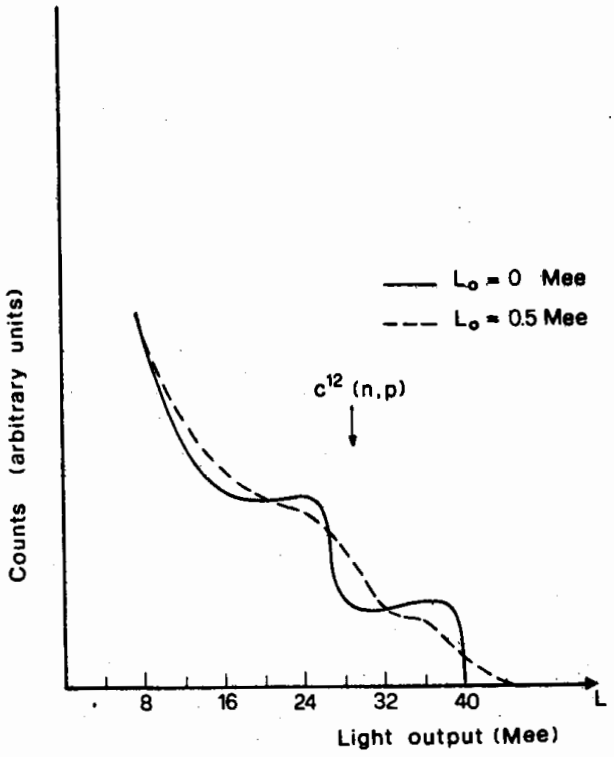

Fig. 5. Effect of the finite resolution on the response function of a NE102 A plastic scintillator (6.35 cm × 30.5 cm) at $E_n = 50$ MeV.

E_{ext} has been evaluated from R_{ext}, using the energy range curves, and the energy loss $\Delta E = E - E_{ext}$ directly computed. The detected pulse height $L(\Delta E) = L(E) - L(E_{ext})$ has been finally obtained from fig. 4.

3. Discussion and results

The comparison of the computed response functions with the experimental data requires a folding on the instrumental resolution. The folding has been performed, as suggested in ref. 3, by adding to the light output L a jitter $\pm \Delta L$ randomly chosen from a Gaussian distribution. If we define L_0 as the light output required for the emission of one photoelectron, the standard deviation $\sigma = L_0[(L/L_0)+0.5]^{\frac{1}{2}}$, is proportional to the number of primary photoelectrons, i.e. to the experimental resolution. The photoelectronic level L_0 has been treated as a free parameter as shown in fig. 5.

Another parameter which has to be determined is the ratio h [eq. (6)] between the fast and slow component of the proton spectrum from the (n, p) reactions in ^{12}C. The existence of a non-negligible fast component from the two-body dis-integration $^{12}C(n, p)^{12}B$ * gives rise to a steep increase of the response function at the kinematic (n, p) threshold (fig. 5). Below 60 MeV the relative strength h has been therefore adjusted to fit the response function in NE102A around the (n, p) threshold (fig. 6). Above 60 MeV no detailed response function data are presently available and the efficiencies $\varepsilon(E)$ generally show a weak dependence on h. A constant value $h = 2.4$ is compatible in this energy region with all the analyzed experimental efficiency curves (fig. 7). The fitted h values are reported in table 4 at various incident neutron energies. Linear interpolation of these results has been used to calculate the response functions of liquid scintillators NE218 and NE213 (table 1). The computed

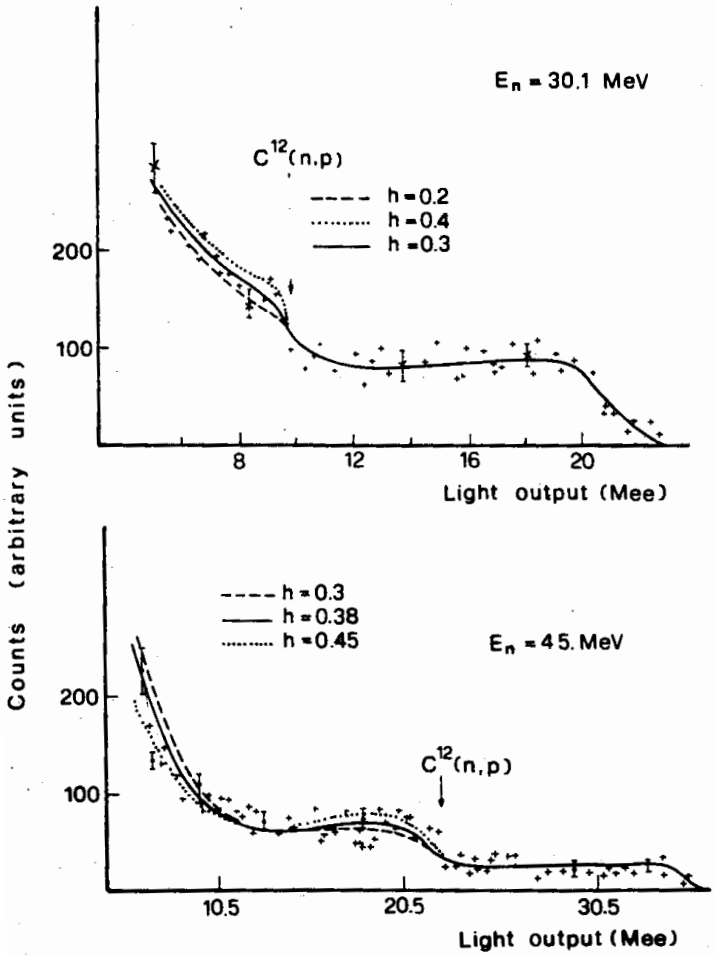

Fig. 6. Response functions[19]) of a cylindrical NE102 A scintillator (8.89 cm × 7.62 cm) at incident neutron energies 30 and 45 MeV. The results of the calculation for different strengths h of the direct two-body $^{12}C(n, p)$ cross section are reported. The photoelectronic level is $L_0 = 0.025$ Mee in both figures.

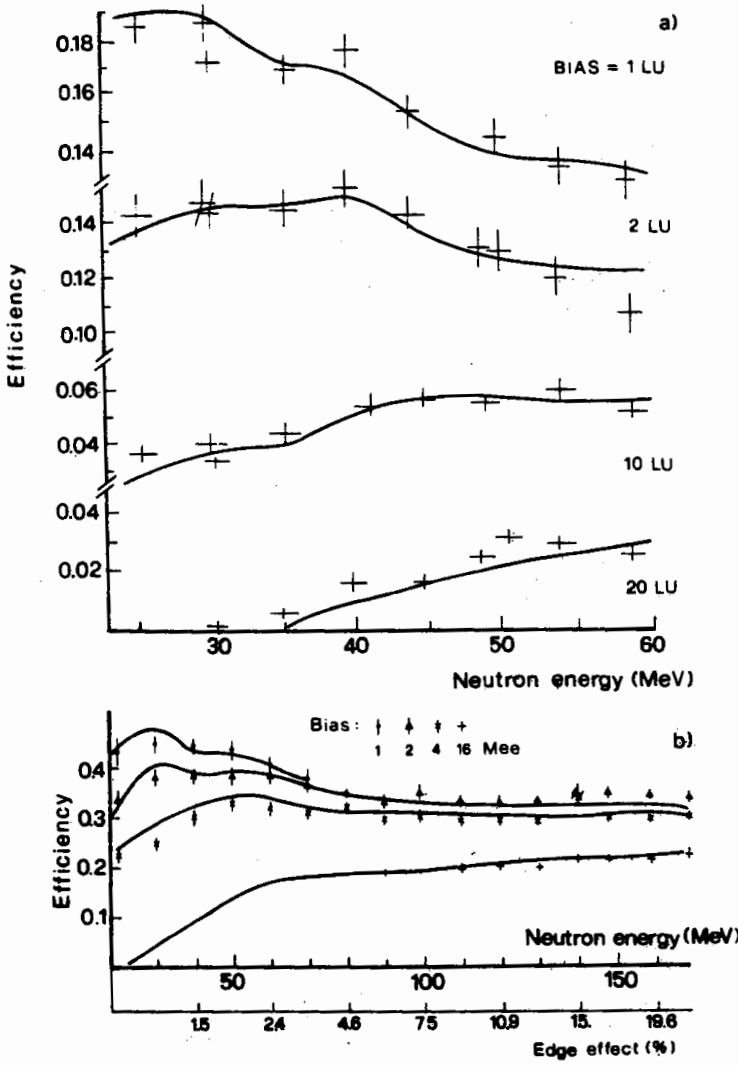

Fig. 7. Computed efficiency curves in different NE102 A scintillators as a function of the neutron energy. Data points are from (a) a (8.89 cm × 7.62 cm) detector[19]), (b) a (6.35 cm × 30.5 cm) detector[20]). The lower scale in (b) represents the percentage of neutron histories showing, at various energies, the edge effect.

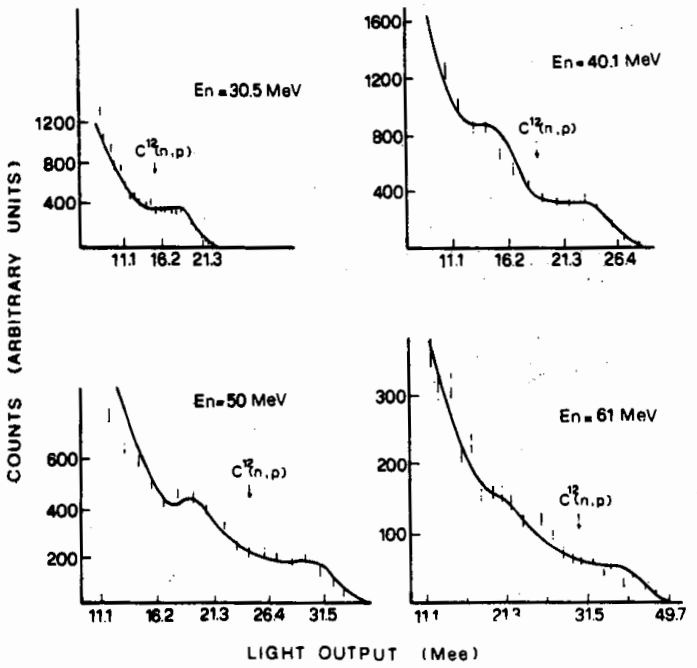

Fig. 8. Response functions[6]) of a cylindrical NE218 scintillator (2.54 cm × 7.62 cm) at various incident neutron energies. The result of our calculation with $L_0 = 0.05$ Mee is given by the full curve.

curves (figs. 8, 9) generally show fair agreement with the experimental data over the whole measured light output range.

We can therefore conclude that the Monte Carlo method is adequate to describe the neutron response functions in most scintillators at least up to 60 MeV, provided that an accurate choice of the experimental neutron cross section data is performed. At higher energies the reliability of the calculation is still limited by the poor knowledge of the $^{12}C(n, p)$ and $^{12}C(n, d)$ cross sections. Nevertheless a correct evaluation of the efficiency, at least at low threshold values, can still be obtained using the analysis of table 4.

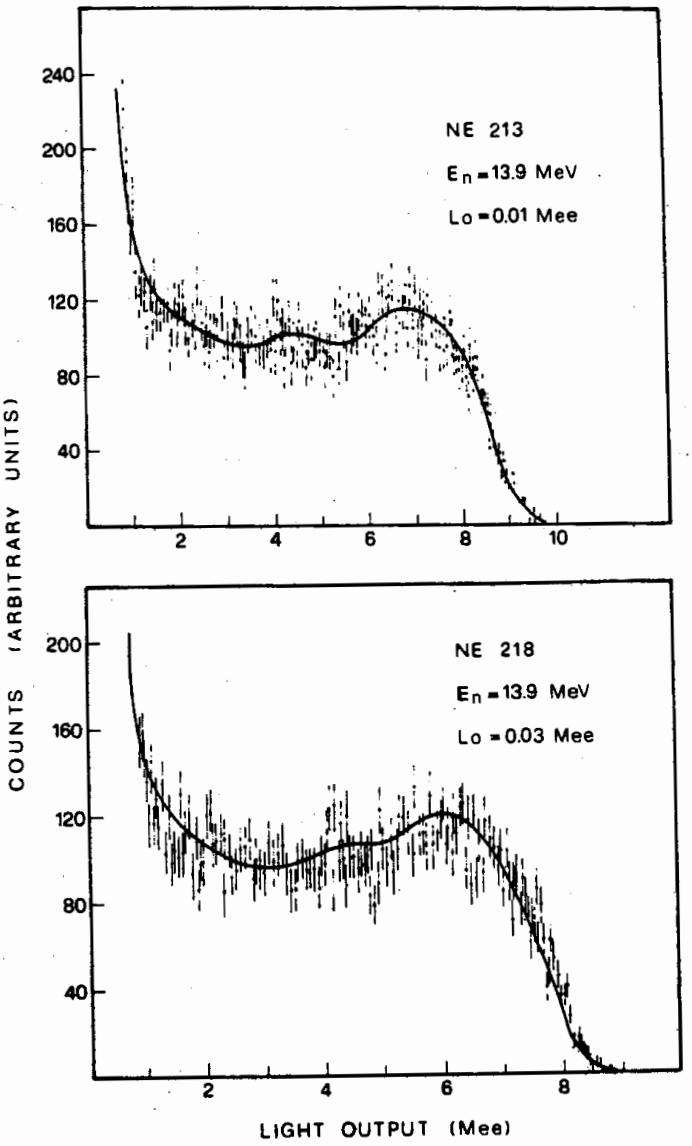

Fig. 9. Response function[21]) of a cylindrical NE213 (6.35 cm × 12.7 cm) and NE218 (6.35 cm × 12.7 cm) scintillator at $E = 19.9$ MeV obtained using an axial point source at $z = 40$ cm and a collimation angle $\theta = 0.054$ rad. The full curve is the result of the Monte Carlo calculation.

References

1) W. Jones and M. Toms, NRL Report 7324 (1970).
2) R. J. Kurz, UCRL-11339 (1964).
3) N. R. Stanton, COO-1545-92 (1971).
4) R. De Leo, G. D'Erasmo, A. Pantaleo and G. Russo, Nucl. Instr. and Meth. **119** (1974) 559.
5) A. Del Guerra, Nucl. Instr. and Meth. **135** (1976) 337.
6) J. W. Watson and R. G. Graves, Nucl. Instr. and Meth. **117** (1974) 541.
7) M. Thumm, Z. Physik **A278** (1976) 77.
8) E. D. Cashwell and J. Everett, *A Monte Carlo method for random walk problems* (Pergamon Press, New York, 1959).
9) J. R. Stehn, M. D. Goldberg, B. A. Magurno and R. Wiener-Cashman, BNL-325, vol. 1, 2nd ed., Suppl. 2 (May 1964).
10) R. W. Peelle, Phys. Rev. **105** (1957) 1311.
11) H. Tyren and T. Maris, Nucl. Phys. **4** (1957) 637.
12) H. Kitazawa and N. Yamamuro, J. Phys. Soc. Japan **26** (1969).
13) G. M. Frye, L. Rosen and L. Stewart, Phys. Rev. **99** (1955) 1375.
14) M. W. Mc Naughton, N. King, F. Brady and J. Ullmann, Nucl. Instr. and Meth. **129** (1975) 241.
15) D. A. Kellog, Phys. Rev. **90** (1953) 224.
16) D. Blanc, *Physique nucléaire* (Masson, Paris, 1973).
17) V. V. Verbinski, W. R. Burrus, T. A. Love, W. Zobel and N. W. Hill, Nucl. Instr. and Meth. **65** (1968) 8.
18) T. G. Masterson, Nucl. Instr. and Meth. **88** (1970) 61.
19) R. A. J. Riddle, G. H. Harrison, P. G. Roos and M. J. Saltmarsh, Nucl. Instr. and Meth. **121** (1974) 445.
20) F. P. Brady, J. A. Jungermann, J. C. Young, J. L. Romero and P. J. Symonds, Nucl. Instr. and Meth. **58** (1968) 57.
21) F. Garibaldi and S. Frullani (Istituto Superiore di Sanità, Rome), private communication.